Contour ProtégéAI™

WHITE PAPER

Automated Contouring Using Neural Networks

Hanlin Wan, PhD
MIM Software Inc., Cleveland, OH, United States

Introduction

Automated segmentation of structures on medical images has always been challenging. In clinical practice, much of the segmentation is performed manually, which is highly time-consuming. Many semi- and fully-automated algorithms have been developed to aid physicians in contouring, such as thresholding[1], edge detection based methods[2], deformable models[3], and atlas-based registration[4].

However, many structures have various textural and intensity patterns, making it almost impossible for any single computer vision-based algorithm to work effectively in a universal fashion. In recent years, research on the use of neural networks has grown rapidly. The performance of these networks on many computer vision tasks has often surpassed that of a human, such as in image classification tasks like ImageNet[5].

Contour ProtégéAI™ provides a neural network framework for automated contouring of normal structures on CT and MR images. The same framework will also be expanded to segment lesions and/or structures on other modalities in the future.

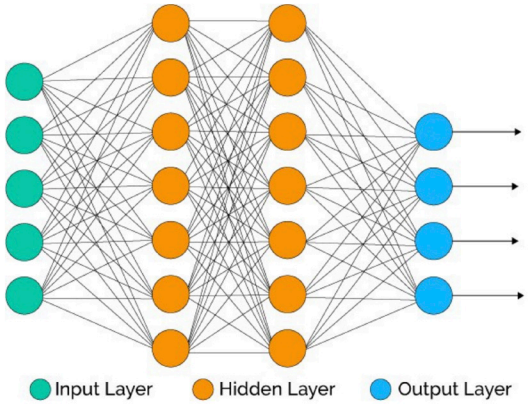

Figure 1 Schematic of a basic neural network

Neural networks attempt to mimic how the human brain works. The brain consists of billions of neurons. Each neuron receives multiple signals from other neurons and sends out a signal based on those inputs. These neurons are often organized into layers, allowing the brain to use simple building blocks to process complicated input signals. Figure 1 shows an example of a basic neural network. Each line has a weight and an associated bias.

Therefore, the nodes calculate a weighted sum of its inputs and then applies some activation function. The output is then sent to the next node until the final output layer is reached. When training a neural network, pairs of inputs and desired outputs are shown. The network learns to adjust the network parameters to minimize the difference between its outputs and the desired outputs. Essentially, neural networks learn to recognize patterns much in the same way the human brain does. This pattern learning is what makes neural networks so powerful, allowing them to exceed the performance of traditional methods.

Contour ProtégéAI's neural network model is based on the U-Net architecture, which has been used for segmentation in numerous different applications. The model consists of many layers of weights and biases as mentioned above to transform the input image to a segmentation mask for each structure at the final output layer. This output is then post-processed to keep the single, largest connected component.

Training and Validation

A large, multi-institution dataset was assembled for training. To establish the performance of the models, five-fold cross-validation was performed. A stratified sampling scheme was used, in which data from each institution was split evenly between the folds, with 10 random datasets per institution withheld to verify the model performance. The mean and standard deviation of the model performance among the five folds was then calculated.

Results

Two metrics were used to compare the ground truth contours to the network outputs: Dice coefficient and mean distance to agreement (MDA). The Dice coefficient measures the spatial overlap between the ground truth and the neural network segmentation. The MDA is the average of the closest distance between all points on the boundaries of the ground truth and neural network output.

Table 1 shows the mean and standard deviation of Dice coefficients and MDA in millimeters (mm) for the 48 structures in CT models. Table 2 shows the same statistics for the three structures in the MR model.

Figures 2 and 3 show boxplots of the range of Dice coefficients for each structure. Figures 4 and 5 compare the mean Dice of the neural network and MIM Software's atlas using majority vote 5. In all cases, Contour ProtégéAI's neural network segmentations were proportionate or superior to atlas-based segmentation.the atlas-based segmentation.

Structure	Mean Dice	Std Dice	Mean MDA (mm)	Std MDA (mm)
Bladder	0.93	0.05	1.30	1.30
Bone_Mandible	0.88	0.06	1.87	5.53
Bowel	0.69	0.19	7.73	8.86
BrachialPlex_L	0.49	0.15	4.12	4.39
BrachialPlex_R	0.48	0.15	4.75	4.95
Brain	0.97	0.02	1.06	0.77
Brainstem	0.84	0.08	1.77	1.10
Breast_L	0.83	0.06	3.75	2.13
Breast_R	0.82	0.06	3.89	1.58
Carina	0.73	0.20	1.98	3.14
Cavity_Oral	0.73	0.16	4.72	3.04
Cochlea_L	0.63	0.16	1.22	0.67
Cochlea_R	0.64	0.17	1.17	0.65
Colon_Sigmoid	0.62	0.28	5.81	8.19
Cricoid	0.73	0.13	1.38	1.30
Esophagus	0.72	0.14	4.36	7.99
Eye_L	0.89	0.08	0.81	0.48
Eye_R	0.89	0.08	0.81	0.45
Femur_L	0.92	0.06	1.66	1.67
Femur_R	0.91	0.08	1.96	3.48
Glnd_Submand_L	0.80	0.14	1.28	0.95
Glnd_Submand_R	0.79	0.13	1.28	0.73
Glnd_Thyroid	0.71	0.17	2.69	2.71
Heart	0.89	0.06	3.63	2.70
Kidney_L	0.93	0.07	1.23	0.87
Kidney_R	0.93	0.06	1.23	0.91
Larynx	0.75	0.15	2.94	1.86
Lens_L	0.70	0.16	0.66	0.38
Lens_R	0.69	0.15	0.66	0.35
Lips	0.70	0.14	2.18	1.55
Liver	0.94	0.07	2.10	2.69
Lung_L	0.96	0.04	1.38	2.61
Lung_R	0.96	0.04	1.46	3.66
Musc_Constrict	0.72	0.08	1.30	0.59
OpticChiasm	0.44	0.17	1.90	0.85
OpticNrv_L	0.63	0.11	1.09	0.59
OpticNrv_R	0.64	0.11	1.07	0.60
Pancreas	0.82	0.07	1.54	1.07
Parotid_L	0.81	0.09	1.85	0.98
Parotid_R	0.80	0.11	2.03	2.21
PenileBulb	0.62	0.17	2.33	2.32
Pituitary	0.62	0.17	0.99	0.45
Prostate	0.84	0.08	1.99	0.94
Rectum	0.83	0.07	2.43	1.85
SeminalVes	0.71	0.15	2.03	1.67
SpinalCord	0.81	0.10	2.21	5.52
Stomach	0.87	0.08	2.55	2.48
Trachea	0.77	0.11	2.91	2.30

Table 1 Dice and MDA for the 48 CT structures.

Structure	Mean Dice	Std Dice	Mean MDA (mm)	Std MDA (mm)
Prostate	0.94	0.03	0.89	0.43
SeminalVes	0.70	0.12	1.69	0.96
Urethra	0.57	0.16	1.90	1.84

Table 2 Dice and MDA for the 3 MR structures.

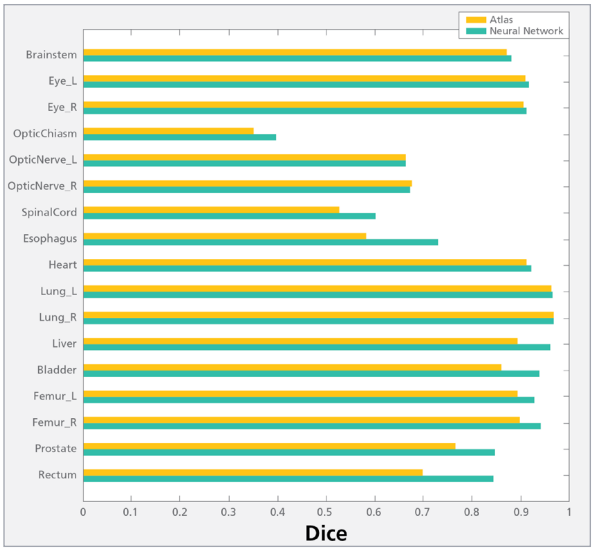

Figure 4 Comparison of NN and atlas dice on CT.

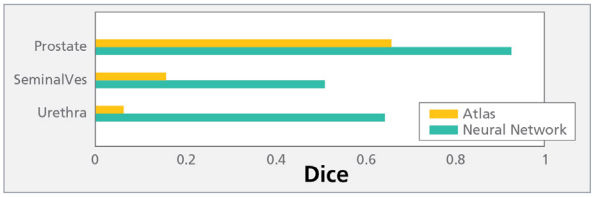

Figure 5 Comparison of NN and atlas dice on MR.

MIM Software Inc. • 25800 Science Park Drive - Suite 180, Cleveland, Ohio 44122 • 866-421-2536

References

1. Weszka, J. S. (1978). A survey of threshold selection techniques. Computer Graphics and Image Processing, 7(2), 259-265.

2. Senthilkumaran, N., & Rajesh, R. (2009). Edge detection techniques for image segmentation-a survey of soft computing approaches. International journal of recent trends in engineering, 1(2), 250.

3. McInerney, T., & Terzopoulos, D. (1996). Deformable models in medical image analysis: a survey. Medical image analysis, 1(2), 91-108.

4. Klein, S., Staring, M., Murphy, K., Viergever, M. A., & Pluim, J. P. (2010). Elastix: a toolbox for intensity-based medical image registration. IEEE transactions on medical imaging, 29(1), 196-205.

5. Russakovsky, O., Deng, J., Su, H., Krause, J., Satheesh, S., Ma, S., ... & Berg, A. C. (2015). Imagenet large scale visual recognition challenge. International journal of computer vision, 115(3), 211-252.

MIM Software Inc. • 25800 Science Park Drive - Suite 180, Cleveland, Ohio 44122 • 866-421-2536